LASER
& PHOTONICS
REVIEWS

Supporting Information

for *Laser Photonics Rev.*, DOI 10.1002/lpor.202401714

Experimental Emulator of Pulse Dynamics in Fractional Nonlinear Schrödinger Equation

Shilong Liu, Yingwen Zhang, Stéphane Virally, Ebrahim Karimi, Boris A. Malomed and Denis V. Seletskiy**

Supplementary information: Experimental emulator of pulse dynamics in fractional nonlinear Schrödinger equation

Shilong Liu,[1,2,*] Yingwen Zhang,[1,3] Stéphane Virally,[4] Ebrahim Karimi,[1,3] Boris A. Malomed,[5,6] and Denis V. Seletskiy[4,†]

[1]*Department of Physics, University of Ottawa, 25 Templeton Street, K1N 6N5, Ottawa, ON, Canada*

[2]*Tempo Optics Inc., Montréal, Québec H3T 1W9, Canada*

[3]*National Research Council of Canada, 100 Sussex Drive, K1A 0R6, Ottawa, ON, Canada*

[4]*femtoQ Lab, Engineering Physics Department, Polytechnique Montréal, Montréal, Québec H3T 1J4, Canada*

[5]*Department of Physical Electronics, Faculty of Engineering, and Center for Light-Matter Interaction, Tel Aviv University, Tel Aviv 69978, Israel*

[6]*Instituto de Alta Investigación, Universidad de Tarapacá, Casilla 7D, Arica, Chile*

[*] dr.shilongliu@gmail.com

[†] denis.seletskiy@polymtl.ca

Section 1: The definition of the fractional dispersion length

The fractional dispersion length is an effective index for evaluating the variance for the pulse duration under the action of the fractional dispersion. To define it, we first perform a simulation for the evolution along z for the pulse's temporal intensity under the fractional group-velocity dispersion (F-GVD) with LI $\alpha = 1$. The intensity is plotted in Fig. 1(a), where we set the half pulse duration $T_0^{\alpha=1}$ ($1/e$ intensity point) to be 1 ps. The corresponding $T_0^{\alpha=1}$ is displayed at the bottom of Fig. 1(a). Here, the pulse duration broadens $\sqrt{2}$ times than the initial value, which is around 1.41 ps, at z is $\sim$ 101 m. This value can be defined as the dispersion length $L_{\alpha=1,\mathrm{FDL}}$. By calculations of the dispersion length vs. α from 0 to 2, we plot it by blue dots in Fig. 1(b), where the solid line is based on the analytical relation:

$$L_{\alpha,\mathrm{FDL}} = \frac{2T_0^{\alpha}}{|D|\alpha}, \qquad \alpha \in (0, 2]. \tag{1}$$

Here, D is the fractional dispersion coefficient, which can be set to $-21 \times 10^{-3}\mathrm{ps}^{\alpha}/\mathrm{m}$. When $\alpha = 2$, $L_{\alpha,\mathrm{FDL}}$ amounts to the well-known GVD dispersion length [1]. Figure 1(c) yields the dispersion length $L_{\alpha,\mathrm{FDL}}$, for the initial pulse with a duration of 0.353 ps, which is close to the observed pulse duration in the experimental setup. The results produced by Eq. 1 agree well with numerical simulations. It should be noted that the pulse dynamics for the fractional dispersion are quite different from the case of regular dispersion. For example, the pulse will split into two lobes under the largely fractional dispersion. The fractional dispersion is only used to evaluate the extension of pulse profiles.

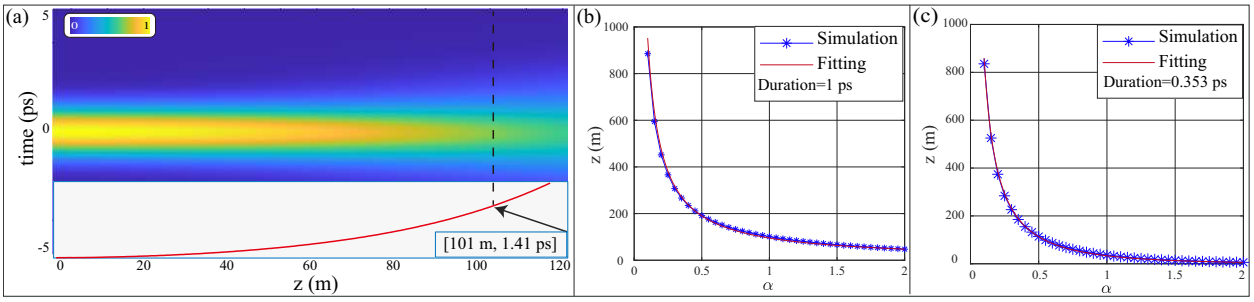

FIG. 1. The definition of the fractional dispersion length. (a): The dynamics of the pulse temporal intensity along z, under the fractional GVD with LI $\alpha = 1$. The corresponding half pulse duration $T_0^{\alpha=1}$ (at the $1/e$ intensity point) is inserted at the bottom of (a), where the pulse duration is around 1.41 ps, and the corresponding dispersion length is around 101 m. (b): The dispersion length versus LI α varying from 0 to 2, where the blue data gives values from the simulation for the initial pulse with duration 1 ps, and the solid line corresponds to the results of the analysis. (c): The results for the initial pulse with duration 0.353 ps.

Section 2: The pulse reconstructions for intra-cavity by the collinear FROG

Using the built collinear Frequency-Resolved Optical Gating (FROG) system [2–4], we have reconstructed the temporal profiles emitted from the mode-locked fiber cavity (MLF), which is also the case of intra-cavity. As detailed in Figure 2(a) of the main text, we aimed to measure the pulse emitted from a stable MLF while employing a pulse shaper with a hologram defined by the Lévy index (LI, α) and dispersion distance (L_{dis}). The α was varied from 0 to 2, and L_{dis} was adjusted to approach the boundary between stability and instability as closely as possible.

These results are displayed in Fig. 2. In this figure, the top panel shows the reconstructed spectral amplitude (blue line) and phase (red line). The corresponding temporal profiles are presented in the bottom panels. Notably, sub-oscillation structures are evident at the bottom of the pulse, particularly in cases involving fractional phase settings. This characteristic is corroborated by the dips observed in the spectral amplitude, consistent with the spectrum acquired from the Optical Spectrum Analyzer (OSA), confirming the alignment of the spectrum between the reconstructions and observations.

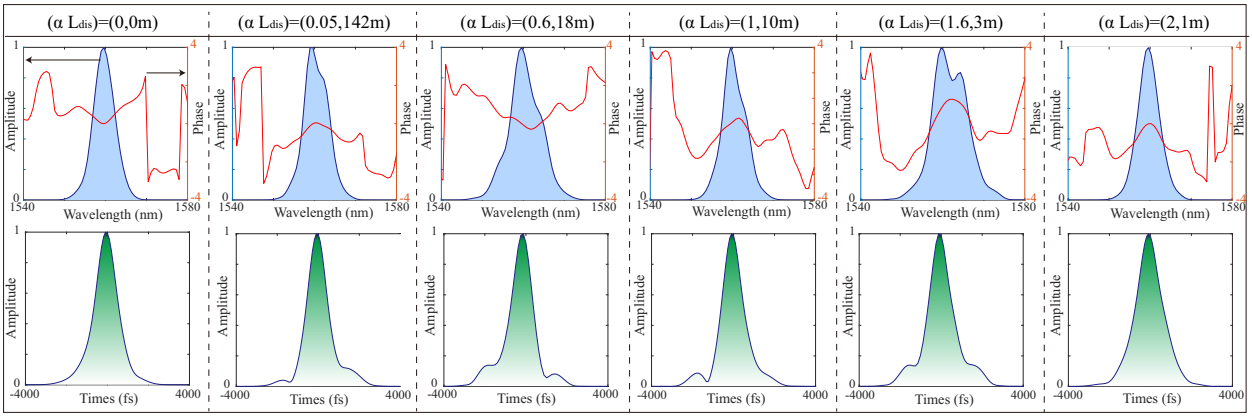

FIG. 2. The reconstructed spectral and temporal amplitudes by the collinear FROG system. The LI α in hologram is set from 0 to 2, with the dispersion distance L_{dis} that is labeled at the top of panels.

Section 3: The setup of extra-cavity to produce spectral valley

The experimental setup used in this work consists of a passive mode-locked fiber (MLF) laser as the source of soliton pulses, as depicted in Figure 3(a). Approximately 25% of the laser pulse is extracted from the output coupler (OC), resulting in a femtosecond soliton pulse with a bandwidth of approximately 4.7 nm, a central wavelength of approximately 1560 nm, and a repetition frequency of approximately 16.65 MHz. The soliton pulse is then directed to a pulse shaper (PS) via a collimator (P1), where a spatial light modulator (SLM) is employed to load a hologram for dispersion engineering. This hologram allows manipulations with regular and fractional dispersion. Next, the output laser pulse is coupled by P2 and directed into the erbium-doped fiber to perform self-phase modulation (SPM) that also includes a segment the of single-mode fiber (SMF). This part serves a dual purpose, amplifying the pulse energy and facilitating SPM. A tunable 980 nm pump laser is utilized to adjust the nonlinear strength, referred to above as the B value. Approximately 90% of the laser pulse, output from P4, is measured using techniques such as frequency-resolved optical gating (FROG) or time-stretch Dispersion Fourier transform (TS-DFT) systems. Meanwhile, the remaining 10% of the laser pulse is monitored in the spectrum by an optical spectrum analyzer.

The pulse shaper, as shown in Figure 3(b), is responsible for achieving a desired pulse shape within the temporal window, given by $\Psi_{\text{out}}(t) = \mathcal{F}^{-1}[M(\omega)\tilde{\Psi}_{\text{in}}(\omega)]$. Here, $M(\omega)$ represents the frequency transfer function that is loaded onto the spatial light modulator (SLM) using a hologram, utilizing the spatial frequency dispersion relation [5]. In this experiment, we only employ the phase shaping and a spectral filter, without the amplitude modulation that could decrease the collecting efficiency [4, 5]. To prevent zero-order crosstalk in the course of the pulse shaping, a spatial grating is superposed onto the phase profile [6].

To verify the imprinted spectral phase onto the initial pulse, a FROG system, as shown in Figure 3(d), is built. The FROG utilizes a collinear structure [4] with a type-II BBO (β-Barium borate) crystal. The output signal $A_{\text{SFG}}(t)$ can be approximately expressed as $A_{\text{SFG}}(t) \sim \chi A_V(t)A_H(t-\tau)$ after the sum frequency generation (SFG), where χ represents the strength of the nonlinear interaction. By arranging a tunable polarization interferometer, no additional loss is introduced besides the transmission losses. The signal after SFG is then directed to a spectrometer for spectrum measurements, in which an optical grating, lens, and charge-coupled device (CCD) camera are addressed.

In addition to the FROG, we have also implemented a time-stretching DFT system for spectrum measurements in a single-shot manner. This system has two purposes –the optical signal transmission and real-time measurement of the spectral intensity. It consists of two sections: the first one is approximately 200 m long dispersion-compensating fiber (DCF) with a second-order GVD coefficient ($\beta_2 \sim -57.1 \times 10^{-3}\text{ps}^2/\text{m}$). The second section is a standard single-mode fiber (SMF) with a length of around 100 km. This arrangement allows rapid stretching of the pulse in the first

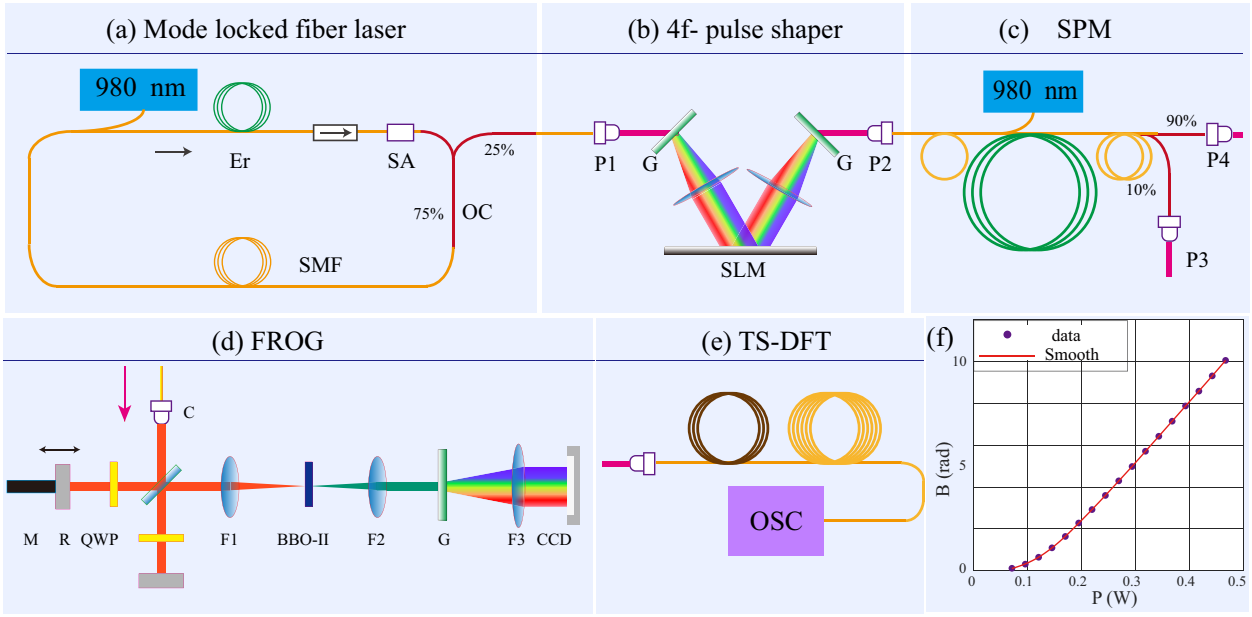

FIG. 3. The setup for the realization of the spectral valley. (a): The passive mode-locked fiber laser. It includes a 980 nm pump laser, isolator, saturable absorber (SA), $\sim$ 1 m Er-doped fiber, $\sim$ 10 m single mode fiber, and an output coupler (OC) with a ratio of 25:75. (b): The pulse shaper. Two symmetric optical gratings (940 grooves/mm) and lens (focus length $\sim$ 150 mm) are aligned at two sides of SLM (Santec SLM-100: 1440$\times$1050 pixels). (c): The SPM. It includes an Er-doped gain fiber ($\sim$ 1.1 m), tunable 980 pump power, as well as a segment of SMF. (d): The FROG. The collinear FROG setup includes a 1mm long type-II (o+e$\rightarrow$e) BBO crystal, a tunable polarization interferometer, and a spectrometer made of CCD (IDS camera) and an optical grating (1200 grooves/mm). (e): The time-stretching dispersion Fourier transform (TS-DFT). It includes two segments of a dispersion chromatic fiber ($\sim$ 200 m with $\beta_2 = -57.1 \times 10^{-3}\mathrm{ps}^2/\mathrm{m}$) and 100 km single-mode fiber. The output is measured by an oscilloscope (OSC). (f): The measured relation between the value of *B* and pump power in the SPM system.

section, which helps to reduce nonlinearity effects in the subsequent SMF section [1, 7–9].

In Fig. 3(f), we present the relationship between the value of *B* and pump power in the SPM system, as shown in Fig. 3(c). To measure it, we first fix the hologram in the SLM and ensure that the soliton pulse passes through the SPM system. Then, we scan the pump power P_{pump} from approximately 70 to 480 mW and record the output average power via port 3 in Fig. 3(c). By considering the relationship between the average power and the pulse peak power [1], we obtain the peak power P_k. Taking into account the length of the erbium-doped fiber $L \sim 1.1$ m and the nonlinear Kerr coefficient $\gamma \sim 0.0032$, we establish an approximate relationship between the value of *B* and the pump power, given by $B = \gamma L P_k(P_{\mathrm{pump}})$. We have also added a smooth line to represent these data in Fig. 3(f). It is observed that *B* and the pump power approximately follow a linear relationship.

Section 4: The pulse reconstructions for extra-cavity by the collinear FROG

Figure 4 presents the outcomes of FROG measurements performed within an extra-cavity setup, capturing various aspects of pulse characterization. The figure includes the FROG trace, temporal intensity, spectrum intensity, and the reconstructed spectral phase. The hologram employs a second-order spectral phase, denoted as L_2.

Panel (a) depicts the scenario where L_2 is set to zero, indicating that the hologram carries a flat phase. In this configuration, the pulse duration, T_0, measures approximately 0.857 ps. The reconstructed profile reveals the presence of a second-order spectral phase, which originates from the group delay dispersion (GDD) introduced by the optical fibers and lenses during transmission. Adjustments in the pulse shape may involve compensating for GDD or higher-order dispersion effects.

To compensate for the additional GDD, a second-order spectral phase can be incorporated in advance. Panel (d) illustrates the condition achieving the minimum pulse duration of about 353 fs, where L_2 is adjusted to approximately -10 m. The pulse durations recorded for varying L_2 values are [0.857 ps, 0.708 ps, 0.467 ps, 0.353 ps, 0.522 ps] corresponding to L_2 settings of [0, 5 m, 8 m, 10 m, 17 m], respectively.

Simulations performed to model these scenarios yielded pulse durations of [0.692 ps, 0.462 ps, 0.373 ps, 0.353 ps, 0.545 ps] for the same L_2 settings, with the minimum duration also set at 0.353 ps. Although there is a slight discrepancy between the experimental and predictions, potentially due to unaccounted higher-order GVD, these findings highlight the significant impact of the second-order phase on pulse duration.

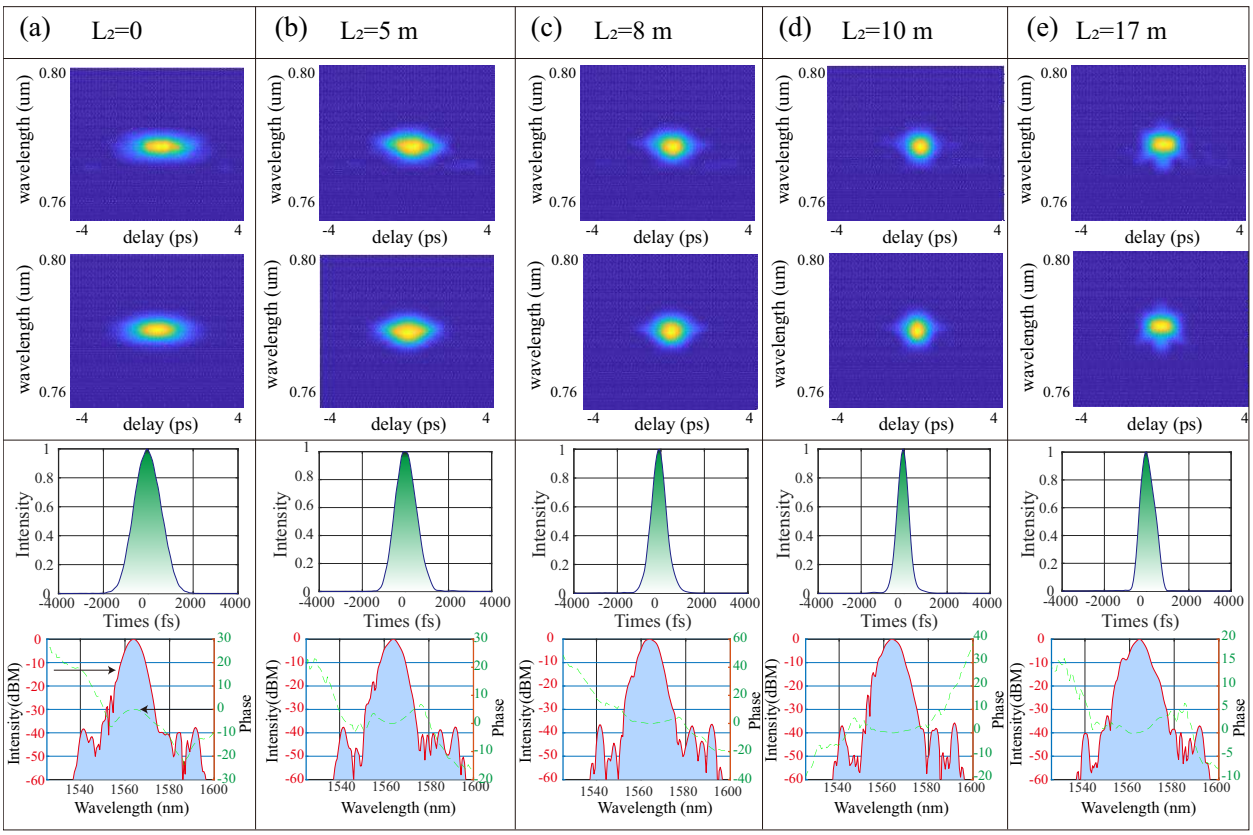

FIG. 4. The results for the FROG. (a): The measured FROG trace, experimental FROG trace, temporal intensity, and spectral intensity, as well as the reconstructed spectral phase. Here, the second-order phase, represented by L_2, is set to zero, which means the hologram in SLM has a flat phase. (b)-(e): Results for L_2 taking values 5m, 8m, 10m, and 16m, respectively.

Section 5: Removal of the Kelly band in soliton pulses

The presence of Kelly sidebands in the soliton pulse's spectral intensity (SI) as depicted in Fig. 5(a1) requires pre-removal to prevent spectral crosstalk [9, 10]. This was accomplished by incorporating a bandpass filter into the hologram design, highlighted in a green area in Fig. 5(b1), where the fractional phase is set as $[\alpha, z] = [1, -3.87 \times L_{\alpha,F}]$. The filter effectively eliminates the Kelly sidebands of the spectrum, demonstrated in Fig. 5(c1). For comparison, we perform two measurements in SI with and without the filter by scanning the pump power. The corresponding SI are shown in Fig. 5(b2) and (c2), respectively, where the pump power is scanned from 70 to 350 mW. Fig. 5(a2) illustrates one dimensional normalized SI for a pump power of around 250 mW, as marked by the dashed white line in Fig. 5(b2) and (c2). These results depict that the existence of Kelly sidebands would make the crosstalk on the spectral lobes. And, the inserted frequency filter could remove them during the spectral dynamics in nonlinear medium.

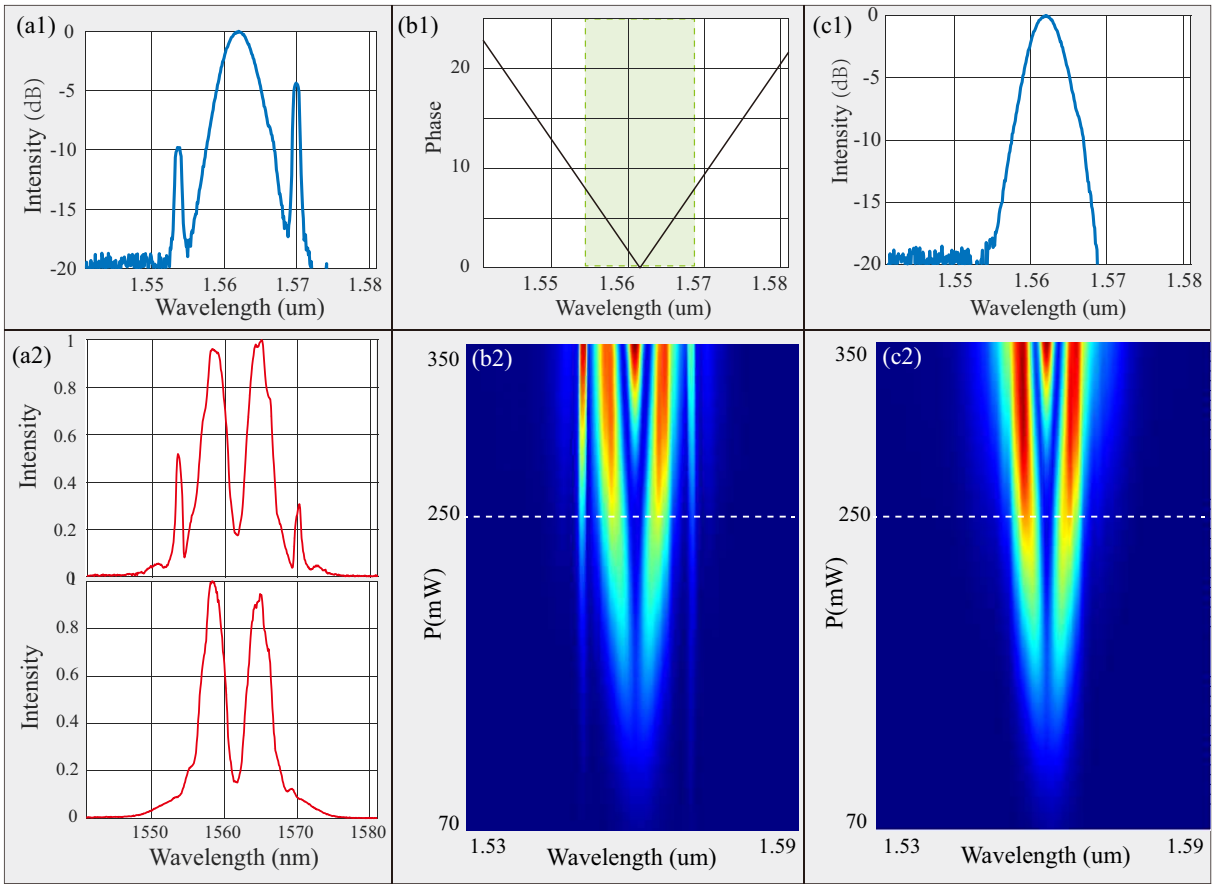

FIG. 5. The functions of Kelly sidebands in spectral intensity (SI) under the SPM. (a1): the SI of the soliton pulse emitted from a mode-locked fiber laser. (a2): the fractional phase of $[\alpha, z] = [1, -3.87 \times L_{\alpha,F}]$ and the frequency filter marked by green area. (c1): The measured SI by performing the filter. (a2): one-dimensional normalized SI for a pump power of around 250 mW. (b2)-(c2): the recorded SI with and without the filter by scanning the pump power from 70 to 350 mW.

[1] Govind P Agrawal. Nonlinear fiber optics. In *Nonlinear Science at the Dawn of the 21st Century*, pages 195–211. Springer, 2000.

[2] Rick Trebino, Kenneth W DeLong, David N Fittinghoff, John N Sweetser, Marco A Krumbügel, Bruce A Richman, and Daniel J Kane. Measuring ultrashort laser pulses in the time-frequency domain using frequency-resolved optical gating. *Rev. Sci. Instrum.*, 68(9):3277–3295, 1997.

[3] Ian A Walmsley and Christophe Dorrer. Characterization of ultrashort electromagnetic pulses. *Adv. Opt. Photonics*, 1(2):308–437, 2009.

[4] Shilong Liu, Yudong Cui, Ebrahim Karimi, and Boris A Malomed. On-demand harnessing of photonic soliton molecules. *Optica*, 9(2):240–250, 2022.

[5] Andrew M Weiner. Ultrafast optical pulse shaping: A tutorial review. *Opt. Commun.*, 284(15):3669–3692, 2011.

[6] Shi-Long Liu, Qiang Zhou, Shi-Kai Liu, Yan Li, Yin-Hai Li, Zhi-Yuan Zhou, Guang-Can Guo, and Bao-Sen Shi. Classical analogy of a cat state using vortex light. *Communications Physics*, 2(1):1–9, 2019.

[7] Yuri S Kivshar and Govind P Agrawal. *Optical solitons: from fibers to photonic crystals*. Academic press, 2003.

[8] Angelin Vithya, MS Mani Rajan, and S Arun Prakash. Combined effects of frequency and higher-order effects on soliton conversion in an erbium fiber with inhomogeneous broadening. *Nonlinear Dynamics*, 91:687–696, 2018.

[9] Boris A Malomed. Multidimensional solitons, 2022.

[10] SMJ Kelly. Characteristic sideband instability of the periodically amplified (average) soliton. In *International Quantum Electronics Conference*, page TuH3. Optica Publishing Group, 1992.